










Article

Droplet Microfluidics Enables Tracing of Target Cells at the Single-Cell Transcriptome Resolution

Yang Liu ^{1,†}, Shiyu Wang ^{1,2,†} , Menghua Lyu ^{1,2,†}, Run Xie ³, Weijin Guo ⁴ , Ying He ⁵ , Xuyang Shi ^{1,2}, Yang Wang ¹, Jingyu Qi ¹, Qianqian Zhu ¹ , Hui Zhang ¹, Tao Luo ⁶ , Huaying Chen ⁷, Yonggang Zhu ⁷ , Xuan Dong ¹ , Zida Li ³ , Ying Gu ¹, Longqi Liu ^{1,8,*}, Xun Xu ^{1,9,*} and Ya Liu ^{1,10,*} 

¹ BGI-Shenzhen, Shenzhen 518083, China

² College of Life Sciences, University of Chinese Academy of Sciences, Beijing 100049, China

³ Department of Biomedical Engineering, School of Medicine, Shenzhen University, Shenzhen 518060, China

⁴ Department of Biomedical Engineering, Shantou University, Shantou 515063, China

⁵ Department of Gynaecological Oncology, Cancer Hospital Chinese Academy of Medical Sciences, Shenzhen Center, Shenzhen 518116, China

⁶ Department of Mechanical & Electrical Engineering, Xiamen University, Xiamen 361101, China

⁷ School of Mechanical Engineering and Automation, Harbin Institute of Technology, Shenzhen, Shenzhen 518055, China

⁸ Shenzhen Bay Laboratory, Shenzhen 518000, China

⁹ Guangdong Provincial Key Laboratory of Genome Read and Write, BGI-Shenzhen, Shenzhen 518120, China

¹⁰ Shenzhen Key Laboratory of Single-Cell Omics, BGI-Shenzhen, Shenzhen 518100, China

* Correspondence: liulongqi@genomics.cn (L.L.); xuxun@genomics.cn (X.X.); liuya1@genomics.cn (Y.L.)

† These authors contributed equally to this work.



Citation: Liu, Y.; Wang, S.; Lyu, M.; Xie, R.; Guo, W.; He, Y.; Shi, X.; Wang, Y.; Qi, J.; Zhu, Q.; et al. Droplet Microfluidics Enables Tracing of Target Cells at the Single-Cell Transcriptome Resolution. *Bioengineering* **2022**, *9*, 674. <https://doi.org/10.3390/bioengineering9110674>

Academic Editors: Janina Bahnemann, Sofia Arshavsky-Graham and Max M. Gong

Received: 23 September 2022

Accepted: 7 November 2022

Published: 10 November 2022

Publisher's Note: MDPI stays neutral with regard to jurisdictional claims in published maps and institutional affiliations.



Copyright: © 2022 by the authors. Licensee MDPI, Basel, Switzerland. This article is an open access article distributed under the terms and conditions of the Creative Commons Attribution (CC BY) license (<https://creativecommons.org/licenses/by/4.0/>).

Abstract: The rapid promotion of single-cell omics in various fields has begun to help solve many problems encountered in research, including precision medicine, prenatal diagnosis, and embryo development. Meanwhile, single-cell techniques are also constantly updated with increasing demand. For some specific target cells, the workflow from droplet screening to single-cell sequencing is a preferred option and should reduce the impact of operation steps, such as demulsification and cell recovery. We developed an all-in-droplet method integrating cell encapsulation, target sorting, droplet picoinjection, and single-cell transcriptome profiling on chips to achieve labor-saving monitoring of TCR-T cells. As a proof of concept, in this research, TCR-T cells were encapsulated, sorted, and performed single-cell transcriptome sequencing (scRNA-seq) by injecting reagents into droplets. It avoided the tedious operation of droplet breakage and re-encapsulation between droplet sorting and scRNA-seq. Moreover, convenient device operation will accelerate the progress of chip marketization. The strategy achieved an excellent recovery performance of single-cell transcriptome with a median gene number over 4000 and a cross-contamination rate of $8.2 \pm 2\%$. Furthermore, this strategy allows us to develop a device with high integrability to monitor infused TCR-T cells, which will promote the development of adoptive T cell immunotherapy and their clinical application.

Keywords: T-cell; droplet-based microfluidics; single-cell transcriptome; droplet picoinjection

1. Introduction

Since the implementation of the Human Genome Project in the last century, the popularization of DNA and RNA sequencing technologies has shown tremendous impact on the development of the entire life sciences and medical fields. With the deepening of research, we find substantial differences between thousands of cells in a tissue, and even phenotypically identical cells also have heterogeneity and differences in gene expression levels [1,2]. Therefore, the interpretation of single-cell genetic information provides stronger technical support for cancer treatment, embryonic development, prenatal diagnosis, etc. [3,4]. Because of this, a revolution in single-cell sequencing may rebuild the cognition of cellular life. The rapid evolution of single-cell omics is inseparable from the fast upgrade of application

tools. In 2015, Drop-seq was proposed to set up a bridge between single-cell profiling and high-throughput technology [5] and also laid the foundation for the development of similar tools at a later stage. The introduction of droplet microfluidics also directly stimulates the throughput of single-cell sequencing to increase exponentially, and RNA profiling of millions of cells has been achieved in less than a decade [6].

Without exception, under the mainstream single-cell tools with microfluidics as the technical background [7,8], experimental samples require processes such as single-cell suspension preparation, droplet generation, mRNA capture, demulsification, etc. However, in some specific applications, there is a need to enrich target cells with specific needs from the sample in advance, the subsequent single-cell sequencing process will also have strict requirements on cell input and viability. For instance, engineered T cells equipped with receptors can specifically recognize the antigens on tumor cells [9,10] and then initiate cytotoxic effects to suppress tumors. Sorting and unveiling the phenotypes of T cells pre- and post-infusion will be instructive to uncover their cellular biology and microenvironmental factors underpinnings. Alternatively, by integrating plasma cell encapsulation, antibody secretion screening in droplets, and scRNA-seq into a pipeline on chips, the time for identifying antigen-specific antibodies is compressed to 24 h from weeks [11,12]. Commercialized fluorescence-activated cell sorting (FACS) is preferred for enriching cells and allowing samples to adapt microwell [13] or droplet-based RNA-sequencing [14]. To promote efficiency and convenience, droplet-based microfluidics systems have been developed to handle sorting and single-cell analysis. Recently, the dielectrophoresis array [15] and differential flow resistance principle [16] have improved the cell utilization rate of micro-well chips and increased the capability of handling scRNA-seq for abundant cells. However, the absence of a sorting function makes these methods not always appropriate for target cell scRNA-seq. As a comparison, droplet-based single-cell sequencing has achieved significant breakthroughs in many areas thanks to its high convenience in operation. Importantly, similar fluorescence-based optical sorting methods have been available for years and can induce high efficiency. However, a drawback of existing droplet-based strategies is the inevitable step of sorted droplet breakage and re-encapsulating cells for downstream single-cell sequencing, which would affect the cell viability and total number [11,12].

Herein, we integrated sample preparation based on droplets, target sorting, droplet picoinjection, and single-cell transcriptome profiling to generate an efficient platform for examining TCR-T cells at single-cell resolution (Figure 1A). As a proof of concept, TCR-T cells in a mixture are labeled with fluorescence, and then, cells are co-encapsulated with RNA beads (DNBelab C4) for transcriptome information capture in droplets. For enrichment of TCR-T cells, targets are sorted into a collector, which is compatible with the pico-injector inlet hole based on the activation of fluorescent tags. Negative pressure is transiently applied to the chip, and droplets are driven to the flow channel, where reagents for scRNA-seq are injected into droplets facilitated by an electric field. Afterward, the cells are subjected to lysis inside droplets, transcripts capture, library preparation, and RNA-sequencing.

The pipeline achieves a high-throughput cell sorting rate (up to 450 droplets per second), convenient processes without steps of breaking and re-generating droplets, and ideal quality of single-cell transcriptome (median gene number per cell: ~4000). Then, the cell-cycle phases and other phenotypes of TCR-T cells were presented in a demo, highlighting the potentiality of our strategy for unveiling heterogeneous phenotypes of TCR-T cells. The droplet injection technology involved in this work is actually a crucial step towards the development of a new method for antigen-specific TCR screening. In previous work, we reported the utilization of droplet microfluidics to sort antigen-specific T cells at a single-cell level, which is conducive to the rapid search for TCRs targeting neoantigens [17]. In that study, we must perform demulsification and cell recovery after target screening before the next step of sequencing work. In the identification step, emulsion-breaking will cause significant obstacles to the identification and backtracking of pairing relationships (TCR-Neoantigen). Therefore, we proposed a novel method of linking droplet injection and

single-cell omics to realize it. It also lays the foundation for establishing the recognition mechanism of tumor neoantigens and their specific TCRs from the single-cell transcriptome level. In the future, the strategy can be used for clinical samples to uncover phenotypes relating to favorable prognosis after infusions and provide clues to design more effective therapies (Figure 1B).

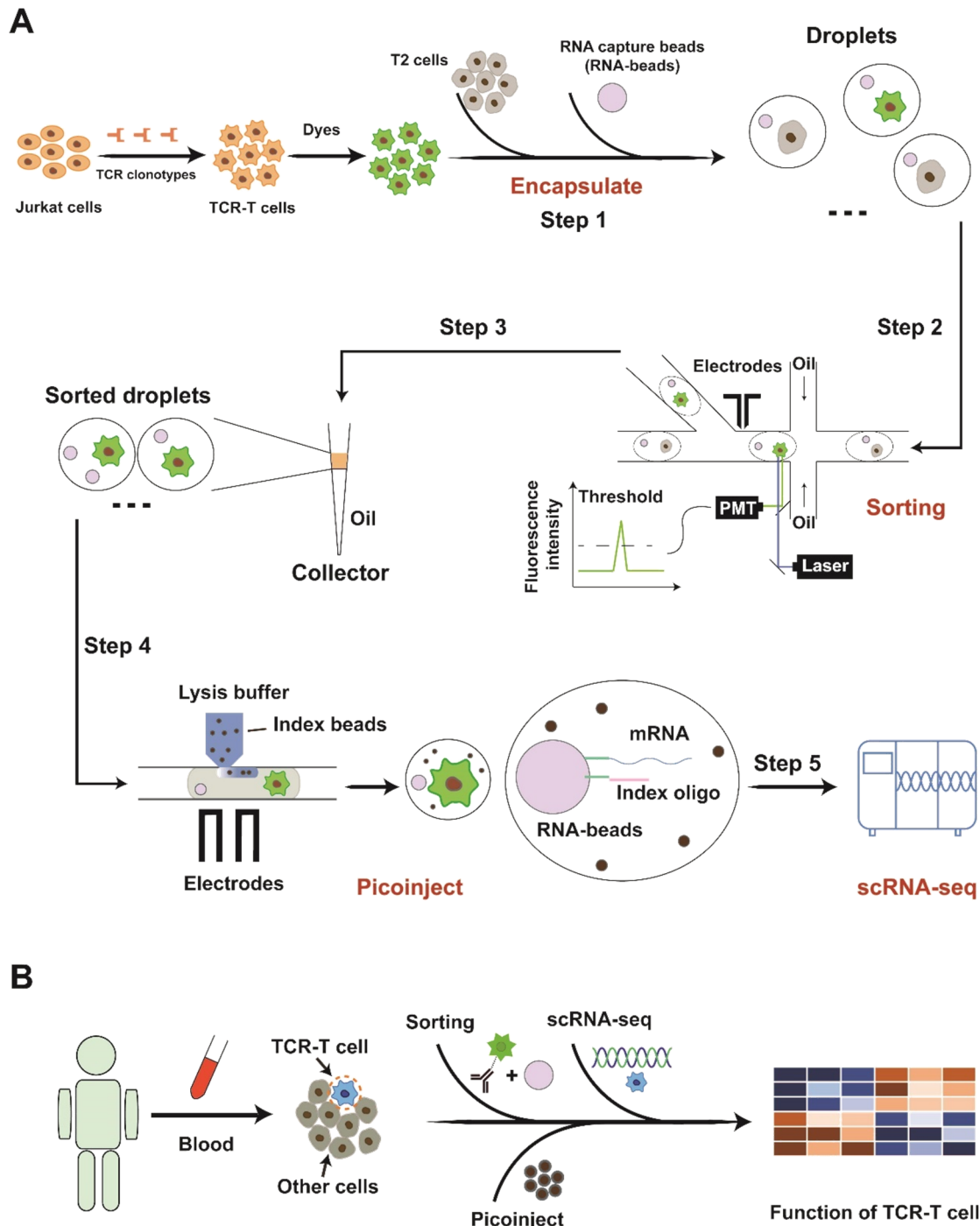


Figure 1. Schematic diagram of experimental flow. (A) Step 1: Droplet generation: Co-encapsulation of cells and RNA beads. Step 2: Droplet sorting: Fluorescence-activated droplet screening and sorting for enriching TCR-T cells. Step 3: Droplet collection; Step 4: Droplet picoinject: Inject reagent (lysis buffer and index beads) into sorted droplet for scRNA-seq. Step 5: Single-cell RNA-sequencing: Capture transcripts, prepare library and perform scRNA-seq. (B) The strategy for monitoring infused TCR-T cells in clinic application.

2. Materials and Experiments

2.1. Chip Design and Fabrication

This study employed AutoCAD to design three different microfluidic chips, including a droplet generation chip (Chip A), a droplet sorting chip (Chip B), and a picoinjection chip (Chip C) (Figure S1). The master models were fabricated using SU-8 photolithography on 4-inch silicon wafers and the chips were fabricated by PDMS as previously described [17]. The channel heights of Chips A, B, and C were 50, 50, and 40 μm , respectively. Given the hydrophobic performance [18], Chip A was bonded on a PDMS-fabricated substrate, Chips B and C were bonded to glass slides after being exposed to oxygen plasma (Harrick plasma cleaner, PDC-002, Ithaca, New York, NY, USA). The details of chip design and fabrication are listed in the Supporting Information and provided as CAD files (CAD-1, CAD-2).

2.2. Cell Culture

T2, Jurkat, NIH/3T3 (CRL-1658), and 293T cell lines were purchased from American Type Culture Collection. The TCR-T cell line was generated by transducing a TCR lentivirus vector into Jurkat cell line as previously described [17]. TCR-T cells and T2 cells were cultured in RPMI 1640 supplemented with 10% (*v/v*) fetal bovine serum (FBS) and 1% penicillin-streptomycin (P/S) at 37 °C with 5% CO_2 . NIH 3T3 and 293T cell lines were cultured in Dulbecco's Modified Eagle Medium (DMEM) supplemented with 10% (*v/v*) FBS and 1% P/S at 37 °C with 5% CO_2 . The details about the main materials were listed in Table S1.

2.3. Cell Staining and Flow Cytometry

TCR-T Cells were washed with DPBS once and resuspended in 1 mL DPBS with 1 μL CellTracker Green CMFDA Dye. After incubation at 37 °C for 30 min, cells were washed 3 times with 1 mL DPBS. Then cells were subsequently centrifuged at $500 \times g$ for 3 min, and resuspended in a working buffer, comprising RPMI 1640 supplemented with 0.1% Pluronic F-68 (diluted from 10% Pluronic F-68), 1% P/S, 100 mM tris(3-hydroxypropyl) phosphine (THPP) and 12% Ficoll PM400 at a final density of 1000/ μL . For flow cytometry (Aria II, BD, San Jose, CA, USA), cells were washed with DPBS twice, centrifuged at $500 \times g$ for 3 min, and resuspended in DPBS with 2% FBS.

2.4. Single-Cell RNA Sequencing

The droplets were incubated for 40 min at room temperature and then demulsified to recover RNA beads. The cDNA library for scRNA-seq was generated by DNBe-lab C4 kit [19]. Then, all libraries were conducted in preparation for DIPSEQ T1 sequencer (MGI). The detailed method for data analysis and data mining are shown in the Supporting Information.

2.5. Statistical Analysis

The statistics were conducted by GraphPad and R. The differences between two groups were examined by the Wilcoxon test, and the *p* values of multiple tests were adjusted by the false discovery rate (FDR) method.

2.6. Data Availability

The data that support the findings of this study have been deposited into CNGB Sequence Archive (CNSA) [20] of China National GeneBank DataBase (CNGBdb) [21] with accession number CNP0002544.

3. Results and Discussion

3.1. Platform Operation

To achieve TCR-T cell enrichment and scRNA-seq based on chips, droplet generation chip (Chip A, Figure S1A,B), droplet sorting chip (Chip B), and picoinjection chip (Chip C, Figure S1C,D) were designed and manufactured in this research. Chip A has two inlets

for samples and one inlet for oil, as well as an outlet for droplets (Figure S1A). The outlet hole of Chip A was connected to a 2 mL collection tube via a polyethylene pipe and the negative pressure driver of 30 mL syringe connected to the outlet of the collecting tube was assembled into a 3D-printed base for supplying force in droplet generation [22]. Then, 50 μ L of bead/cell solution and 400 μ L of oil (1864005, Bio-Rad, Hercules, CA, USA) were added into the individual holes (Figure S1A, Video S1). The negative pressure of \sim 13 kPa as the syringe is pulled up can induce a transient and stable droplet generation, and meanwhile, the overabundant residual in the sample and bead/cell sedimentation in the hole could be effectively avoided. The time for generating millions of droplets was less than 10 min, and no more than 6% pressure decline under the supervision of sensors (4AM01, LabSmith, Livermore, CA, USA) could be contributed (Figure S2A). The syringe operates as a negative pressure pump, and atmosphere pressure promotes liquid and oil flowing into the chip. In the system, the syringe is the only variable to control the droplet dimensions. As shown in our study, the pressure was maintained stable for 10 min, for which one of the main reasons is that the input volume of fluid has little effect on the large volume after pulling the syringe. As presented by other studies, the negative pressure-driven system has a \sim 30% changing broad of droplet diameters [23]. The fluid parameters of chip A were examined by another study, in which the chip exhibited stability to generate droplets of a given size, while its flexibility was limited [22]. Thereby, stability rather than flexibility is significant for chip A.

After droplet generation, we slowly drew the droplet containing oil into a 1 mL syringe with the needle removed. The needle with a pipe infiltrated with oil was installed in this syringe. We turned the syringe slowly until the needle was upward, and then, installed the syringe on the syringe pump. The other end of the pipe was inserted into the droplet inlet of Chip B. Finally, the droplet was reinjected into Chip B by adjusting the flow rate of the syringe pump. For step 1, the entire experimental process took about 15 min, including the time to assemble the device, add reagents and generate droplets. It took about 20 min transferring the generated droplets to Chip B, including the time to draw the droplets into a syringe and test the sorting-related equipment and software. Chip B was adapted from previously published design [17], the droplets and oil input were driven by two independent syringe pumps, and the flow rate was set to 80 and 800 μ L per hour, respectively. When a target droplet was identified, a 20 kHz of 1000 peak-to-peak voltage (\sim 2 ms duration) would be applied to electrodes for cell sorting. In step 2, we took about 15 or 20 min to sort 3000 or 5000 positive droplets, respectively. Next, it took about 10 min to transfer the sorted droplets into the collector and drain the excess oil.

In Chip C, one outlet and three inlets were punched for inputting droplets, oil, and injected reagent, respectively. The entire infusion procedure took approximately 20 min by pulling the syringe from 17 to 20 mL scale, and the negative pressure decay rates were controlled to be 5% (Figure S2B). With the testing of the equipment, the total time we needed to complete step 4 was about 30 min. In this system, injection leakage is an unavoidable phenomenon. The pressure differential between the injector and the oil channel is approximately determined by Laplace pressure [24,25]. However, the picoinjector used herein was driven by negative pressure, suggesting that the pressure in the injector and oil channel were approximately equal to atmospheric pressure, and no differential value was generated. Therefore, this situation eventually led to injection leakages. Instead, connecting injection to a syringe pump may be a feasible manner that could balance the Laplace pressure in turn.

3.2. Cell Encapsulation, Sorting, and Injection

TCR-T was first labeled with CellTracker CMFDA and mixed with T2 cells to mimic cell-type proportions in blood. Then, the CMFDA-stained cells would generate a signal for subsequent droplet sorting. The diameter of droplets for efficiently sorting is required to be 40–60 μ m. To overcome the influence of Poisson distribution as much as possible, the droplet size generated by Chip A was controlled to be \sim 60 μ m. According to the statistics of

7737 droplets, the average diameter of droplets is $56.87 \pm 1.95 \mu\text{m}$ (Figure S3A). In order to verify the stability of the droplets, we put the generated droplets into the incubator for 4 and 6 h, and then counted the diameter distribution of the droplets. Figure S3B,C shows that the droplets did not change significantly in 4–6 h. In this research, subsequent experimental operations could be carried out without incubation after droplet generation, but incubation may be required for 4–6 h after droplet generation in future work. To minimize the possibility of more than one cell in a droplet, cell concentration was adjusted according to Poisson distribution with $\lambda = 0.05$. In Figure S3D, the experimental cell distribution in droplets was approximately determined by Poisson distribution. Therefore, when the cell density was adjusted to $1000/\mu\text{L}$, the rate of droplets with one cell was $4.91 \pm 0.16\%$, and that with more than one cell was $0.13 \pm 0.02\%$, suggesting that the multiplet rate was less than 5%. For common single-cell omics platforms, 5% is an acceptable value balancing intercellular contamination and the amount of available data [26]. In terms of improving cell utilization, RNA beads were over-loaded ($25,000/\mu\text{L}$). Our study showed that the percentage of droplets without RNA bead(s) was about 25% at the bead density of $25,000/\mu\text{L}$. As shown in Figure S3D, the proportion of droplets containing RNA bead(s) was $74.56 \pm 0.53\%$, and $3.70 \pm 0.04\%$ of droplets simultaneously contained RNA bead(s) and cell(s), suggesting that $73.42 \pm 1.59\%$ of droplets encapsulating cells also had beads within (the gray column). Given that only RNA captured by beads could be performed in scRNA-seq, this operation helped us to decrease the loss of cells.

Droplets containing target cells were enriched by the fluorescence-activated droplet sorting (FADS), and in Figure 2A, the fluorescence signal (green) from the CellTracker CMFDA was then accepted and transduced into a voltage signal by a photomultiplier tube (PMT). Additionally, the voltage was simultaneously delivered to a comparator and single-chip microcomputer (SCM). If a voltage exceeded the threshold of the comparator, a high voltage ($\sim 1 \text{ Vpp}$) operating on the full cycle of the PMT signal would be transmitted from the comparator to SCM for triggering PMT signal recording. After the comparator signal ended, the SCM calculated the maximum value of the PMT signal and compared it with the threshold. Thus, a PMT signal above the threshold sent a voltage to sort the droplet by dielectrophoresis. On the contrary, cell-free droplets or non-fluorescent cells did not excite signal peaks (Figure 2B). The approach of droplet sorting finally achieves a percentage of positive cells over 95% re-assessed by flow cytometry (Figure S4), whereas 35% corresponds to the percentage before sorting (Figure 2C).

We connected the outlet catheter to a $200 \mu\text{L}$ pipette tip and added $20 \mu\text{L}$ of empty droplets to prevent further cell loss. Owing to the limited carrying capacity of tip, the tip was inserted into a device whose pressure was operated by a 1 mL syringe for controlling the liquid level, and the detailed procedure is presented in Figure S5. However, there is a risk that the transfer process may influence the uniformity of the droplets, and we also conducted stability statistics of droplets during the transfer from Chip B to Chip C. As we can see in Figure S6A,B, droplet transfer operations have no impact on droplet stability. After sample collection, the pipette tip was then inserted into the inlet on Chip C (Figure 3A), and index beads were resuspended in the lysis buffer at a density of $70,000/\mu\text{L}$ as the injection phase to ensure that each droplet contained index beads after injection. In Figure 3B, droplets and inject solutions were dyed with red and green pigments to facilitate observation, respectively. Following the completion of the color-dye injection, the orange color of droplets reflected a given action. Two distributions of droplets are presented in Figure 3C, in which the uniform values of small (green, $51.22 \pm 3.51 \mu\text{m}$) and large ones (orange, $79.31 \pm 6.23 \mu\text{m}$) indicate the stability of the injector. After incubation at room temperature for 40 min in the collection tube, cells in droplets were lysed, index was cut by reagent, and released mRNA and index were captured by RNA beads (Figure 3D). In order to further explore the stability of droplets, we made statistics on the diameter of droplets before and after incubation (Figure S6C,D). Through statistical calculation, it was found that the diameter distribution of droplets did not change significantly after 40 min of incubation, which confirmed that the incubation process had no effect on droplet stability. Finally,

with droplet breakage, RNA beads were recovered for library preparation as previously described [17]. Figure S7A shows the principle of nucleic acid capture by RNA beads, and Figure S7B shows the distribution of cDNA and oligo after separation and purification, which is consistent with the results of conventional library construction. This indicates that the library can be used for subsequent single-cell sequencing and data analysis.

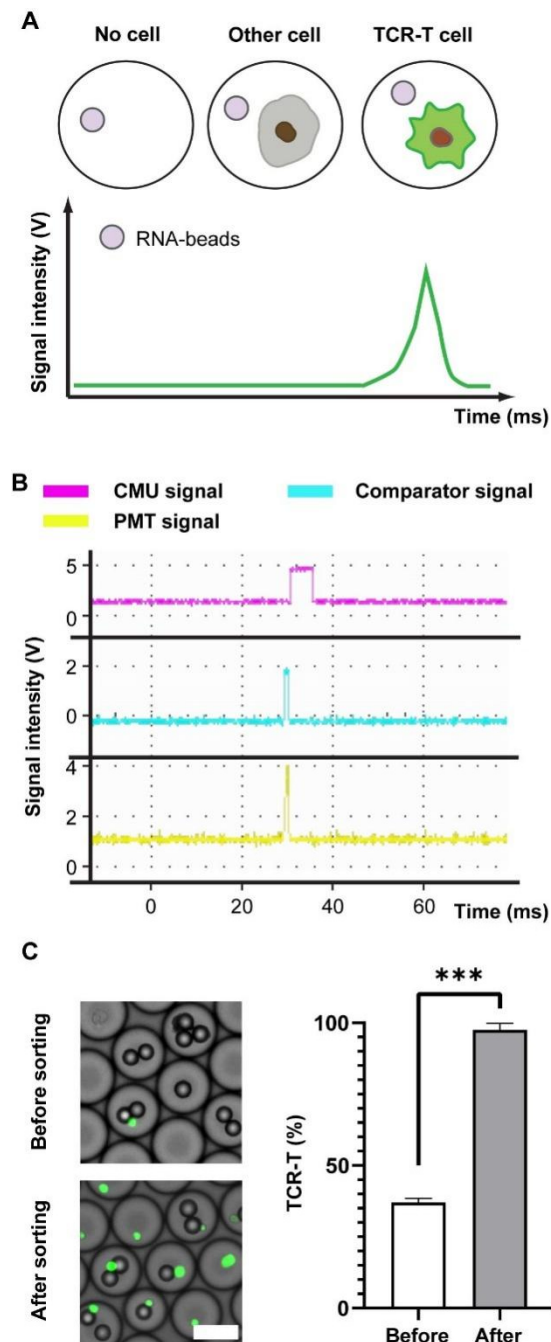


Figure 2. Droplets sorting and signal analysis. (A) The signaling patterns of droplets with cell-free, off-target-cell, or TCR-T cell. (B) A signal recording of droplets with TCR-T cell and feedback signals from comparator and CMU against a positive droplet. (C) Images of droplets before and after sorting (left) and the percentage of CMFDA+ cells detected by flow cytometric analysis. The TCR-T cells are highlighted by green points. Scale bar: 50 μ m. Wilcoxon test is used, and *** $p < 0.001$. *** represents a significant difference.

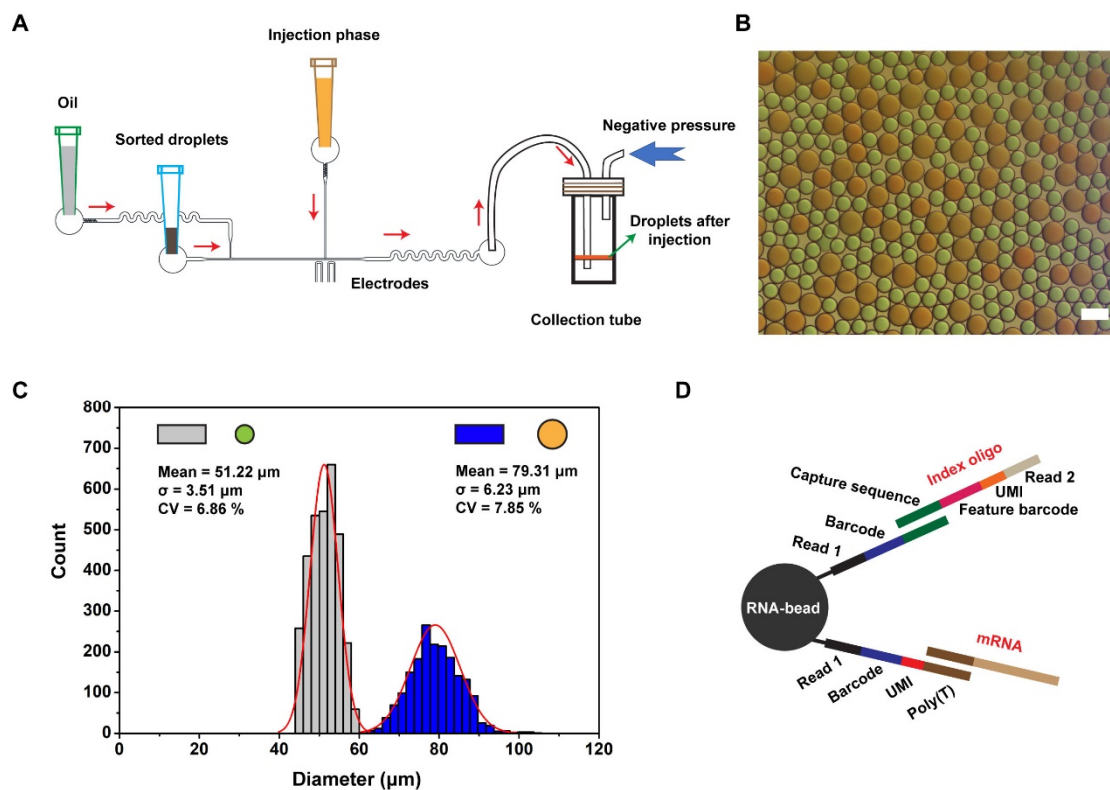


Figure 3. Droplet picoinjection and oligo design for RNA beads. **(A)** The schematic diagram of droplet picoinjection. Negative pressure drives oil, droplets, and injection reagent to flow through channels. Oil controls the distance between two adjacent droplets, and additional reagents are injected into droplets facilitated by an electric field. **(B)** The photograph of droplets after injection. To facilitate observation, droplets and injection were dyed with red and green, respectively, and then red droplets were orange, and leakage droplets of injection were green after injection. Scale bar is 100 μm. **(C)** Diameter distribution of droplets (N = 3203, grey bar; N = 1870, blue bar). **(D)** RNA and index are captured by RNA beads with different capture handles. Sequence structure for capturing index: Bead, read1, barcode, and capture sequence. For capturing RNA: bead, read1, barcode, UMI, and poly(T).

3.3. Data Analysis for Single-Cell Sequencing

3000 and 5000 TCR-T cells were sequentially sorted for picoinjection and scRNA-seq library preparation. After accomplishing the above-mentioned steps, the raw data were aligned and annotated by the PISA pipeline. After normalizing sequencing depth to that of 10X V3 demo, the gene number of 3000- and 5000-cell samples were 3484 ± 300 and 4046 ± 154 , respectively, and the two groups (3000 and 5000-cell samples) did not have obvious differences in UMI and mitochondrial genes rate (Figure 4A). Thereby, the factor of cell number did not affect the gene detection in this method, and the gene number detected here was better than the majority of common scRNA-seq methods [27,28] (Figure 4B). However, the recovery rate of 3000-cell was less than that of 5000-cell samples (Figure 4A). To further explore the problem of cell recovery rate, we have provided a set of experiments (1000-cell samples). In Figures S8 and 4A, we found that the trend was not consistent when the cell input was reduced to 1000. This is because when the number of samples is reduced, the RNA beads input would also be decreased. In subsequent operations, experiments that rely on magnetic bead recovery may cause fluctuations in cell recovery rates due to some experimental errors. To overcome these limitations in the future, performing reverse transcription-PCR [29,30] in droplets and/or replacement of RNA beads with dissolvable material [31,32] and then recovering RNA or cDNA solution may further increase the recovery rate.

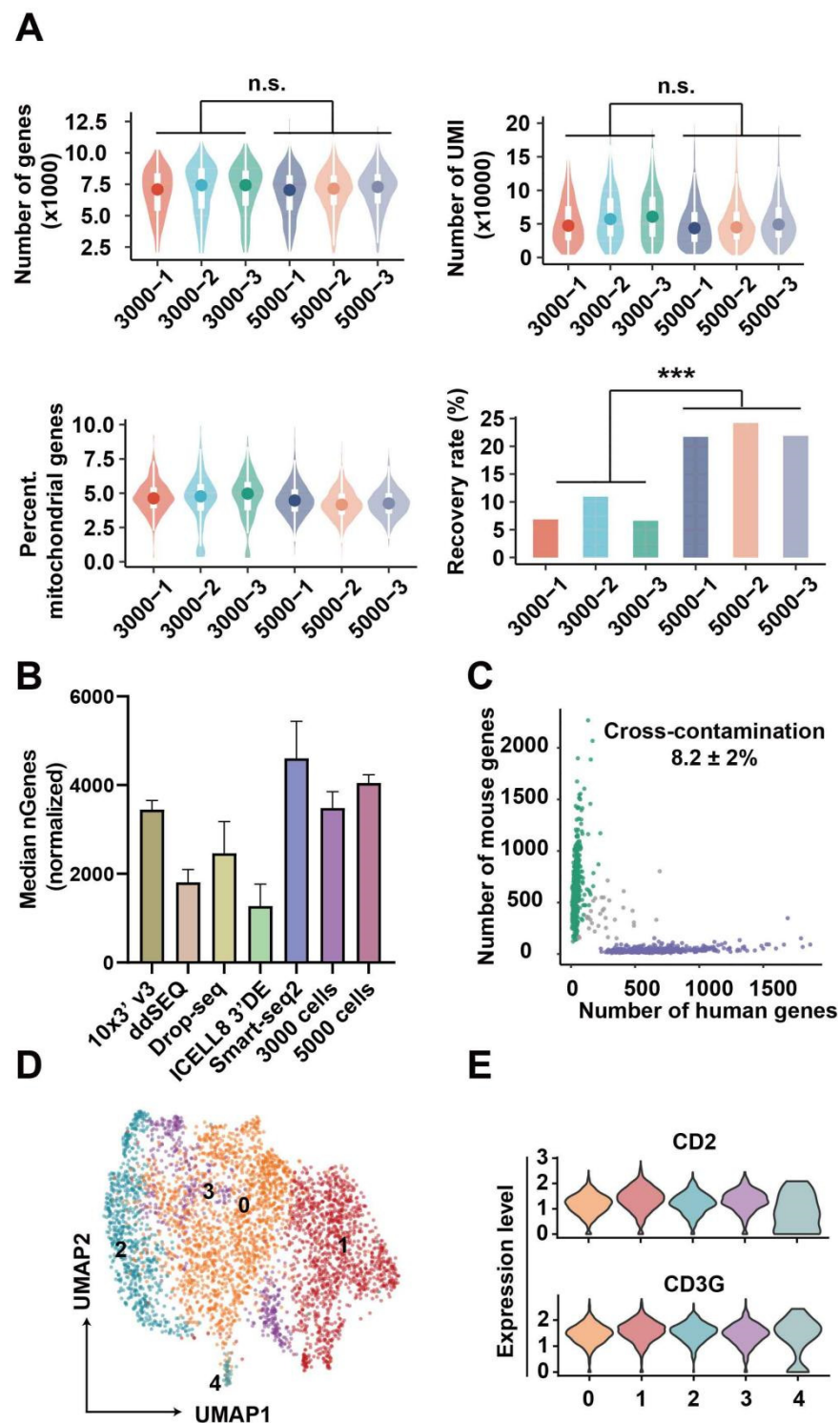


Figure 4. Quality of scRNA-seq data. (A) From the upper to lower, the number of genes per cell (1st), UMI per cell (2nd), and the percentage of mitochondrial genes per cell (3rd), and cell recovery rate (4th). *** represents a significant difference. (B) The median of genes per cell generated by other methods and our method. The gene numbers of 10X, ddSEQ, Drop-seq, ICell8 and our method were adjusted by read number to normalize sequencing depth. (C) The number of genes of human or mouse in each cell. (D) UMAP of cell clusters when SNN graph was construed with a resolution = 1. The numbers 0 to 4 represent five distinct cell subsets. (E) Features markers of TCR-T cells.

To estimate the cross-contamination, 293T (human origin) and NIH 3T3 (mouse origin) cells were equally mixed together for scRNA-seq by our method, and the cross-contamination rate in Figure 4C was $8.2 \pm 2\%$. According to previous reports, the cross-contamination detected by scRNA-seq data was biased from the theoretical value predicted by the Poisson distribution [33]. As shown by Yang et al. [34], ambient RNA released in the cell suspension is a notable factor increasing cross-contamination. Likely, undergoing apoptosis and stressed cells may release these RNA molecules to cell suspension, which are further incorporated in droplets. Beyond ambient RNA, other experimental factors, such as barcode swapping, may also cause cross-contamination [35]. Reducing cell concentration should be efficient in repressing multiplet, and some algorithms can facilitate the detection of varied types of pollution [34,35]. In addition, cells from all samples were distributed evenly on a two-dimension UMAP plot, and the result in Figure S9 reflected that batch effects were adjusted sufficiently. Cells were grouped into five clusters with a resolution = 1 of SNN (Figure 4D), and strong CD2 and CD3G expressions in all clusters (Figure 4E) demonstrated that features of the cellular transcriptome profile can be preserved by this method.

TCR-T cells in vivo can present heterogeneous phenotypes due to their diverse phenotypes pre-infusion [36] and the various effects of the microenvironment after infusion [37]. Next, we further examined gene expressions of TCR-T cells indicated by scRNA-seq data proving that it can uncover the heterogeneity of TCR-T cells and the underlying mechanism. By DEG analysis, the top10 feature genes of each cluster were presented in a heatmap (Figure S10A). The *MCM4*, *PCNA*, *RRM2* were highly expressed by cluster 0, *CCNB1* and *CDC20* were over-expressed by cluster 1, and *CDKN2D* was highly expressed by cluster 3. All of these genes are related to the cell cycle. According to the analysis of cell-cycle feature genes (Figure S10B), the result reflected cells were at different phases (Figure S10C). Then, the data of cells were scaled again after regression of cell cycle genes (Figure S10D). For Figure 5A, cell clusters were skewed and presented novel features (Figure 5B). With annotation of DEGs by GO analysis, cluster 3 expressed spindle and kinetochore-related genes, implying that cells in this cluster were ongoing cell differentiation, and vesicle lumen and vacuolar lumen-related genes were highly expressed in Cluster 4. As reviewed by Gutiérrez-Vázquez et al. [38], these lumen systems tightly regulated the exosome and other cellular transportation systems, which in turn affected the cell-cell interactions and cellular functions. The DEGs in cluster 5 were involved in melanosome, and those in cluster 6 participated in ribosome functions. The results of these analyses on DEGs unveiled the heterogeneously cellular functions of TCR-T cells and suggested that our method was sufficient to trace TCR-T cell phenotypes. Alternatively, complicated environments and cell-cell interactions in clinical practices will induce more diverse phenotypes of TCR-T cells in vivo [39], and our method could transfer more information to uncover the skewed functions of infused cells, which, in turn, provide clues to develop the adoptive T cell therapies.

In terms of current studies on TCR-T/CAR-T in vivo, cell expansion, exhaustion, and trafficking are primary parameters used for evaluating the therapy responses, which can be obtained by flow cytometry and cell imaging analyses [39]. Of course, these parameters were also presented by scRNA-seq in our method. Importantly, other effects, such as cell cytotoxicity and cytokine secretion, can also be exhibited by single-cell omics, which would provide more reliable information to generate an accurate model for estimating TCR-T/CAR-T treatment effect. At the beginning of the project, we also considered integrating the different functional units onto one chip. However, the purpose of our platform is not just for one single application scenario, and we expect that several chips with different roles may be freely combined like building blocks to achieve the best effect. The next application point is to rapidly identify the pairing relationship between TCRT and APC cells (Figure S11). We labeled various TCR-T and APC cells with different barcodes and then encapsulated these cells in droplets along with RNA beads. After incubation for a certain time, the APC cell in the droplet would activate corresponding TCR-T cells by presenting specific antigens, resulting in changes in gene expression of relevant activation

pathways. Then, the corresponding barcodes of TCR-T and APC cells were determined by molecular information recovery, library generation, and data analysis. Ultimately, we hope to speed up the identification of tumor neoantigens. We also expect that our platform combines the diverse omics approaches (proteomics, epigenetics) to allow a considerable potential for enhancing the development of cell therapy.

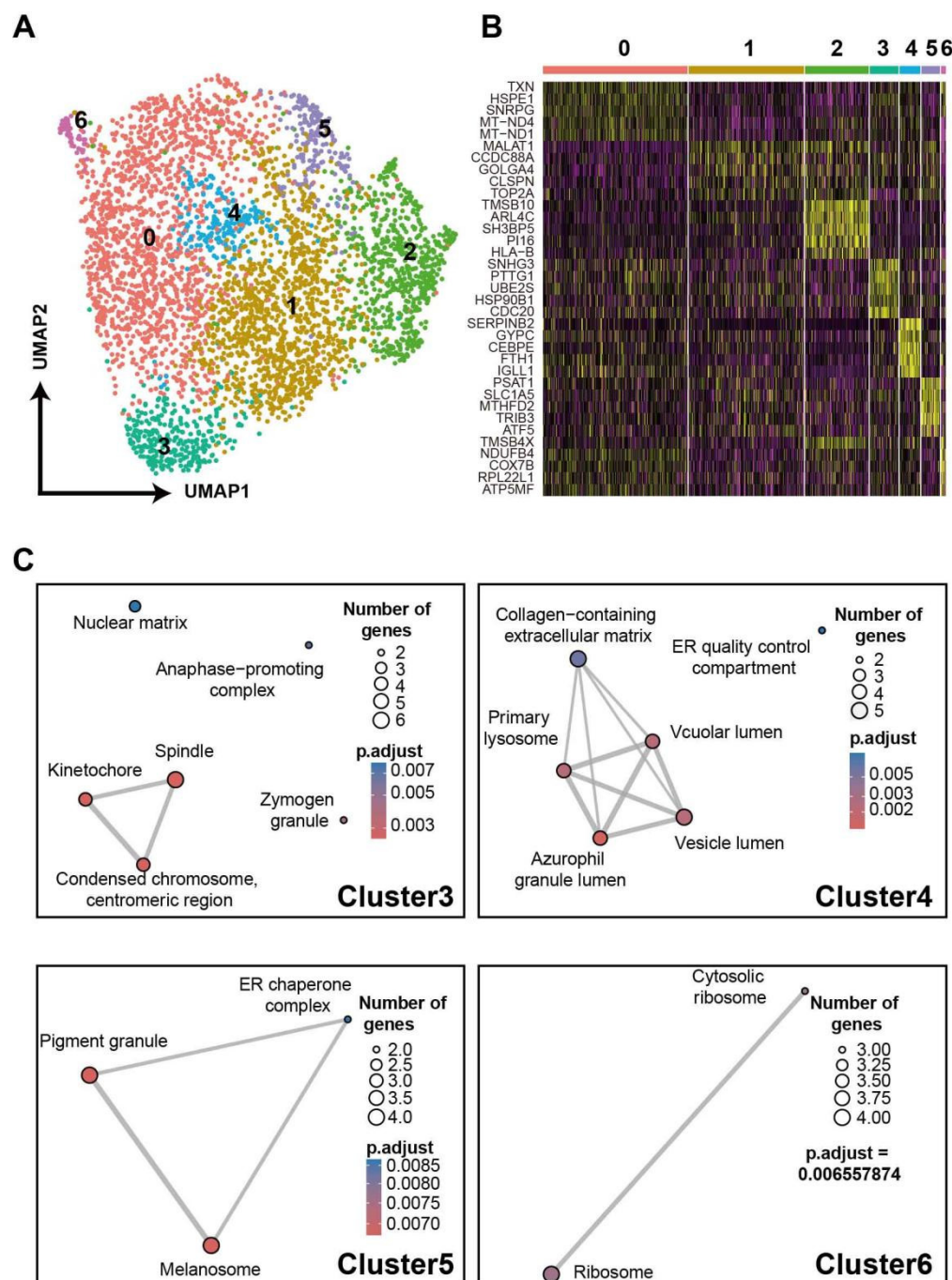


Figure 5. A demo for unveiling TCR-T phenotypes with scRNA-seq data. (A) UMAP of TCR-T cells after cell-cycle regression. The numbers 0 to 6 represent seven distinct cell subsets. (B) Heatmap of top5 DEGs of each subset. (C) GO analyses based on DEGs of each subset.

4. Conclusions

In this study, we developed a strategy with droplet generation, droplet sorting, and picoinjection to integrate cell sorting and single-cell omics. The strategy enriched target cells in a high-throughput manner and performed single-cell omics by injecting reagents into droplets instead of tedious manipulation. This strategy simplifies the pipeline to perform single-cell sequencing for enriched cells and allows further integration of chips to promote cell biology studies and clinical trials. In the future, we can use this strategy to verify the function of TCR-T cells by taking blood from patients and achieve monitoring the infusion of TCR-T cells. This step will promote the development and clinical application of adoptive T cell immunotherapy.

Supplementary Materials: The following supporting information can be downloaded at: <https://www.mdpi.com/article/10.3390/bioengineering9110674/s1>, Figure S1: The detailed design of microfluidic chips; Figure S2: Stability test of negative pressure on microfluidic chips; Figure S3: Statistics of the droplet diameter and encapsulation rate of RNA-beads; Figure S4: Flow cytometry for the identification of TCR-T cells; Figure S5: Sorted droplet collector; Figure S6: Statistics of the droplet diameter on different conditions; Figure S7: Principle and verification of nucleic acid capture; Figure S8: Qualification of 1000-cell samples by RNA sequencing; Figure S9: UMAP of cells from different samples; Figure S10: Cell cycle analyses of TCR-T cells; Figure S11: The strategy of next work in antigen-specific TCR recognition; Table S1: Materials; CAD-1: Droplet sorting chip-Chip B; CAD-2: Picoinjection chip-Chip C; Video S1: Generation of droplets. Reference [40] is cited in the supplementary materials.

Author Contributions: Conceptualization, Y.L. (Ya Liu); methodology, Y.L. (Yang Liu), S.W., M.L., J.Q. and H.Z.; software, M.L., R.X., X.S. and T.L.; validation, Y.L. (Yang Liu) and S.W.; formal analysis, S.W., M.L., R.X., W.G., Y.H., X.S. and Q.Z.; resources, Y.W., H.C. and Y.Z.; data curation, S.W.; writing—original draft preparation, Y.L. (Yang Liu), S.W. and M.L.; writing—review and editing, Z.L. and Y.L. (Ya Liu); supervision, Y.L. (Ya Liu); project administration, Y.L. (Yang Liu); funding acquisition, W.G., X.D., Y.G., L.L., X.X. and Y.L. (Ya Liu). All authors have read and agreed to the published version of the manuscript.

Funding: This research was funded by National Key Research and Development Program of China (2021YFF1200500), Guangdong Basic and Applied Basic Research Foundation (2021A15110459) and Shantou University Scientific Research Foundation for Talents (NTF20034).

Institutional Review Board Statement: Not applicable.

Informed Consent Statement: Not applicable.

Data Availability Statement: Not applicable.

Acknowledgments: Thanks to all the authors for their contributions to this paper.

Conflicts of Interest: The authors declare that they have no known competing financial interests or personal relationships that could have appeared to influence the work reported in this paper.

References

1. Gantner, P.; Pagliuzza, A.; Pardons, M.; Ramgopal, M.; Routy, J.-P.; Fromentin, R.; Chomont, N. Single-cell TCR sequencing reveals phenotypically diverse clonally expanded cells harboring inducible HIV proviruses during ART. *Nat. Commun.* **2020**, *11*, 4089. [\[CrossRef\]](#)
2. Eberwine, J.; Sul, J.-Y.; Bartfai, T.; Kim, J. The promise of single-cell sequencing. *Nat. Methods* **2014**, *11*, 25–27. [\[CrossRef\]](#)
3. Papalexi, E.; Satija, R. Single-cell RNA sequencing to explore immune cell heterogeneity. *Nat. Rev. Immunol.* **2018**, *18*, 35–45. [\[CrossRef\]](#)
4. Guo, X.; Zhang, Y.; Zheng, L.; Zheng, C.; Song, J.; Zhang, Q.; Kang, B.; Liu, Z.; Jin, L.; Xing, R. Global characterization of T cells in non-small-cell lung cancer by single-cell sequencing. *Nat. Med.* **2018**, *24*, 978–985. [\[CrossRef\]](#)
5. Macosko, E.Z.; Basu, A.; Satija, R.; Nemesh, J.; Shekhar, K.; Goldman, M.; Tirosh, I.; Bialas, A.R.; Kamitaki, N.; Martersteck, E.M.; et al. Highly Parallel Genome-wide Expression Profiling of Individual Cells Using Nanoliter Droplets. *Cell* **2015**, *161*, 1202–1214. [\[CrossRef\]](#)
6. Han, L.; Wei, X.; Liu, C.; Volpe, G.; Zhuang, Z.; Zou, X.; Wang, Z.; Pan, T.; Yuan, Y.; Zhang, X.; et al. Cell transcriptomic atlas of the non-human primate *Macaca fascicularis*. *Nature* **2022**, *604*, 723–731. [\[CrossRef\]](#)

7. Zilionis, R.; Nainys, J.; Veres, A.; Savova, V.; Zemmour, D.; Klein, A.M.; Mazutis, L. Single-cell barcoding and sequencing using droplet microfluidics. *Nat. Protoc.* **2017**, *12*, 44–73. [\[CrossRef\]](#)
8. Xu, X.; Zhang, Q.; Song, J.; Ruan, Q.; Ruan, W.; Chen, Y.; Yang, J.; Zhang, X.; Song, Y.; Zhu, Z.; et al. A Highly Sensitive, Accurate, and Automated Single-Cell RNA Sequencing Platform with Digital Microfluidics. *Anal. Chem.* **2020**, *92*, 8599–8606. [\[CrossRef\]](#)
9. Kojima, R.; Scheller, L.; Fussenegger, M. Nonimmune cells equipped with T-cell-receptor-like signaling for cancer cell ablation. *Nat. Chem. Biol.* **2018**, *14*, 42–49. [\[CrossRef\]](#)
10. D'Ippolito, E.; Schober, K.; Nauwerth, M.; Busch, D.H. T cell engineering for adoptive T cell therapy: Safety and receptor avidity. *Cancer Immunol. Immunother.* **2019**, *68*, 1701–1712. [\[CrossRef\]](#)
11. Gerard, A.; Woolfe, A.; Mottet, G.; Reichen, M.; Castrillon, C.; Menrath, V.; Ellouze, S.; Poitou, A.; Doineau, R.; Briseno-Roa, L.; et al. High-throughput single-cell activity-based screening and sequencing of antibodies using droplet microfluidics. *Nat. Biotechnol.* **2020**, *38*, 715–721. [\[CrossRef\]](#)
12. Wang, Y.; Jin, R.; Shen, B.; Li, N.; Zhou, H.; Wang, W.; Zhao, Y.; Huang, M.; Fang, P.; Wang, S.; et al. High-throughput functional screening for next-generation cancer immunotherapy using droplet-based microfluidics. *Sci. Adv.* **2021**, *7*, eabe3839. [\[CrossRef\]](#)
13. Gole, J.; Gore, A.; Richards, A.; Chiu, Y.-J.; Fung, H.-L.; Bushman, D.; Chiang, H.-I.; Chun, J.; Lo, Y.-H.; Zhang, K. Massively parallel polymerase cloning and genome sequencing of single cells using nanoliter microwells. *Nat. Biotechnol.* **2013**, *31*, 1126–1132. [\[CrossRef\]](#)
14. Konstantinides, N.; Kapuralin, K.; Fadil, C.; Barboza, L.; Satija, R.; Desplan, C. Phenotypic Convergence: Distinct Transcription Factors Regulate Common Terminal Features. *Cell* **2018**, *174*, 622–635.e13. [\[CrossRef\]](#)
15. Bai, Z.; Deng, Y.; Kim, D.; Chen, Z.; Xiao, Y.; Fan, R. An Integrated Dielectrophoresis-Trapping and Nanowell Transfer Approach to Enable Double-Sub-Poisson Single-Cell RNA Sequencing. *ACS Nano* **2020**, *14*, 7412–7424. [\[CrossRef\]](#)
16. Zhang, M.; Zou, Y.; Xu, X.; Zhang, X.; Gao, M.; Song, J.; Huang, P.; Chen, Q.; Zhu, Z.; Lin, W.; et al. Highly parallel and efficient single cell mRNA sequencing with paired picoliter chambers. *Nat. Commun.* **2020**, *11*, 2118. [\[CrossRef\]](#)
17. Wang, S.; Liu, Y.; Li, Y.; Lv, M.; Gao, K.; He, Y.; Wei, W.; Zhu, Y.; Dong, X.; Xu, X.; et al. High-Throughput Functional Screening of Antigen-Specific T Cells Based on Droplet Microfluidics at a Single-Cell Level. *Anal. Chem.* **2021**, *94*, 918–926. [\[CrossRef\]](#)
18. Jiang, N.; Wang, Y.; Chan, K.C.; Chan, C.-Y.; Sun, H.; Li, G. Additive Manufactured Graphene Coating with Synergistic Photothermal and Superhydrophobic Effects for Bactericidal Applications. *Glob. Chall.* **2020**, *4*, 1900054. [\[CrossRef\]](#)
19. Liu, C.; Wu, T.; Fan, F.; Liu, Y.; Wu, L.; Junkin, M.; Wang, Z.; Yu, Y.; Wang, W.; Wei, W.; et al. A portable and cost-effective microfluidic system for massively parallel single-cell transcriptome profiling. *bioRxiv* **2019**. [\[CrossRef\]](#)
20. Guo, X.; Chen, F.; Gao, F.; Li, L.; Liu, K.; You, L.; Hua, C.; Yang, F.; Liu, W.; Peng, C.; et al. CNSA: A data repository for archiving omics data. *Database* **2020**, *2020*, baaa055. [\[CrossRef\]](#)
21. Chen, F.Z.; You, L.J.; Yang, F.; Wang, L.N.; Guo, X.Q.; Gao, F.; Hua, C.; Tan, C.; Fang, L.; Shan, R.Q.; et al. CNGBdb: China National GeneBank DataBase. *Yi Chuan* **2020**, *42*, 799–809. [\[PubMed\]](#)
22. Chen, I.-J.; Wu, T.; Hu, S.J.M. A hand-held, power-free microfluidic device for monodisperse droplet generation. *MethodsX* **2018**, *5*, 984–990. [\[CrossRef\]](#) [\[PubMed\]](#)
23. Filatov, N.A.; Evstrapov, A.A.; Bukatin, A.S.J.M. Negative pressure provides simple and stable droplet generation in a flow-focusing microfluidic device. *Micromachines* **2021**, *12*, 662. [\[CrossRef\]](#)
24. Abate, A.R.; Hung, T.; Mary, P.; Agresti, J.J.; Weitz, D.A. High-throughput injection with microfluidics using picoinjectors. *Proc. Natl. Acad. Sci. USA* **2010**, *107*, 19163–19166. [\[CrossRef\]](#) [\[PubMed\]](#)
25. Rhee, M.; Light, Y.K.; Yilmaz, S.; Adams, P.D.; Saxena, D.; Meagher, R.J.; Singh, A.K. Pressure stabilizer for reproducible picoinjection in droplet microfluidic systems. *Lab Chip* **2014**, *14*, 4533–4539. [\[CrossRef\]](#)
26. Wolock, S.L.; Lopez, R.; Klein, A.M. Scrublet: Computational identification of cell doublets in single-cell transcriptomic data. *Cell Syst.* **2019**, *8*, 281–291.e9. [\[CrossRef\]](#)
27. Ding, J.; Adiconis, X.; Simmons, S.K.; Kowalczyk, M.S.; Hession, C.C.; Marjanovic, N.D.; Hughes, T.K.; Wadsworth, M.H.; Burks, T.; Nguyen, L.T.; et al. Systematic comparison of single-cell and single-nucleus RNA-sequencing methods. *Nat. Biotechnol.* **2020**, *38*, 737–746. [\[CrossRef\]](#)
28. Wang, X.; He, Y.; Zhang, Q.; Ren, X.; Zhang, Z. Direct Comparative Analyses of 10X Genomics Chromium and Smart-seq2. *Genom. Proteom. Bioinform.* **2021**, *19*, 253–266. [\[CrossRef\]](#)
29. Kim, S.C.; Clark, I.C.; Shahi, P.; Abate, A.R. Single-cell RT-PCR in microfluidic droplets with integrated chemical lysis. *Anal. Chem.* **2018**, *90*, 1273–1279. [\[CrossRef\]](#)
30. Heijnen, L.; Elsinga, G.; de Graaf, M.; Molenkamp, R.; Koopmans, M.P.; Medema, G. Droplet digital RT-PCR to detect SARS-CoV-2 signature mutations of variants of concern in wastewater. *Sci. Total Environ.* **2021**, *799*, 149456. [\[CrossRef\]](#)
31. Wang, Y.; Cao, T.; Ko, J.; Shen, Y.; Zong, W.; Sheng, K.; Cao, W.; Sun, S.; Cai, L.; Zhou, Y.L. Dissolvable Polyacrylamide Beads for High-Throughput Droplet DNA Barcoding. *Adv. Sci.* **2020**, *7*, 1903463. [\[CrossRef\]](#)
32. Klein, A.M.; Mazutis, L.; Akartuna, I.; Tallapragada, N.; Veres, A.; Li, V.; Peshkin, L.; Weitz, D.A.; Kirschner, M.W. Droplet barcoding for single-cell transcriptomics applied to embryonic stem cells. *Cell* **2015**, *161*, 1187–1201. [\[CrossRef\]](#)
33. Zheng, G.X.; Terry, J.M.; Belgrader, P.; Ryvkin, P.; Bent, Z.W.; Wilson, R.; Ziraldo, S.B.; Wheeler, T.D.; McDermott, G.P.; Zhu, J. Massively parallel digital transcriptional profiling of single cells. *Nat. Commun.* **2017**, *8*, 14049. [\[CrossRef\]](#)
34. Yang, S.; Corbett, S.E.; Koga, Y.; Wang, Z.; Johnson, W.E.; Yajima, M.; Campbell, J.D. Decontamination of ambient RNA in single-cell RNA-seq with DecontX. *Genome Biol.* **2020**, *21*, 57. [\[CrossRef\]](#)

35. Griffiths, J.A.; Richard, A.C.; Bach, K.; Lun, A.T.; Marioni, J.C. Detection and removal of barcode swapping in single-cell RNA-seq data. *Nat. Commun.* **2018**, *9*, 2667. [\[CrossRef\]](#)
36. Tantaló, D.G.M.; Oliver, A.J.; von Scheidt, B.; Harrison, A.J.; Mueller, S.N.; Kershaw, M.H.; Slaney, C.Y. Understanding T cell phenotype for the design of effective chimeric antigen receptor T cell therapies. *J. Immunotherapy Cancer* **2021**, *9*, e002555. [\[CrossRef\]](#)
37. Cazaux, M.; Grandjean, C.L.; Lemaître, F.; Garcia, Z.; Beck, R.J.; Milo, I.; Postat, J.; Beltman, J.B.; Cheadle, E.J.; Bousso, P. Single-cell imaging of CAR T cell activity in vivo reveals extensive functional and anatomical heterogeneity. *J. Exp. Med.* **2019**, *216*, 1038–1049. [\[CrossRef\]](#)
38. Gutiérrez-Vázquez, C.; Villarroya-Beltrí, C.; Mittelbrunn, M.; Sánchez-Madrid, F. Transfer of extracellular vesicles during immune cell-cell interactions. *Immunol. Rev.* **2013**, *251*, 125–142. [\[CrossRef\]](#)
39. Sakemura, R.; Can, I.; Siegler, E.L.; Kenderian, S.S. In vivo CART cell imaging: Paving the way for success in CART cell therapy. *Mol. Ther.-Oncolytics* **2021**, *20*, 625–633. [\[CrossRef\]](#)
40. Wu, T.; Hu, E.; Xu, S.; Chen, M.; Guo, P.; Dai, Z.; Feng, T.; Zhou, L.; Tang, W.; Zhan, L. clusterProfiler 4.0: A universal enrichment tool for interpreting omics data. *Innovation* **2021**, *2*, 100141. [\[CrossRef\]](#)